ISBN: 978-3-95450-132-8 doi:10.18429/JACoW-IPAC2014-TUPME042

PLANNED HIGH-GRADIENT FLAT-BEAM-DRIVEN DIELECTRIC WAKEFIELD EXPERIMENTS AT THE FERMILABÕS ADVANCED SUPERCONDUCTING TEST ACCELERATOR *

F. Lemery[1], D. Mihalcea[1], P. Piot[1,2], and J. Zhu[2,3]
Department of Physics, and Northern Illinois Center for Accelerator & Detector Development, Northern Illinois University DeKalb, IL 60115, USA
[2] Accelerator Physics Center, Fermi National Accelerator Laboratory, Batavia, IL 60510, USA
[3] Institute of Fluid Physics, CAEP, Mianyang 621900, China

Abstract

In beam driven dielectric wakefield acceleration, high-gradient short-wavelength accelerating fields can be achieved with dielectric lined waveguides (DLWs) with small apertures. In this paper we investigate the possibility of using a low-energy (50 MeV) flat beam to excite high-gradient wakefields in a slab-symmetric DLW. We demonstrate via numerical simulation that field amplitudes of > 100 MV/m can be attained using the experimental setup available in the injector of the Advanced Superconducting Test Accelerator (ASTA) currently in its commissioning phase at Fermilab.

INTRODUCTION

The ASTA facility is described elsewhere in these Proceedings [1, 2]. The main attributes of the facility are an L-band (1.3-GHz) superconducting linear accelerator, a high-brightness photoinjector [3], and the inclusion of advanced phase space manipulations such as flat-beam generation [4] and transverse-to-longitudinal exchange [5]. One applications of ASTA is to explore alternative acceleration schemes based on collinear beam-driven methods including dielectric-wakefield acceleration [6] and channeling-acceleration [7] methods.

This paper discusses our efforts to develop an experiment aimed at exploring beam-driven acceleration using slab symmetric DLWs. A large advantage of slab-symmetric DLWs over more conventional cylindrical-symmetric DLWs is the tunability of the inner aperture. Additionally, the flexibility in flat beam generation at the ASTA facility allows us to investigate the use of smaller aperture structures with higher fundamental frequencies which may lead to larger accelerating gradients. Although the experiment focusses on dielectric wakefield acceleration (DWFA), the experimental techniques and setup developed will be used by other advanced-acceleration schemes planned at ASTA.

EXPERIMENTAL SETUP

The beamline configuration for our DWFA experiment is diagrammed in Fig. 1. The beamline comprises a L-band RF gun followed by two SCRF accelerating cavities (CAV1 and 2). The RF gun is nested in a pair of solenoidal lenses that can be used to produce beam with large angular momentum. Such a beam can be decoupled by a set of three skew quadrupole magnets downstream of CAV2 to produce flat beams – beams with high transverse emittance ratio – that can then be compressed using a magnetic chicane (BC1). The skew quadrupole magnets insertion is referred to as round-to-flat-beam transformer (RFBT). Downstream of BC1, a triplet is used to focus the beam inside the DLW structure mounted in a 2-axis goniometer; additionally, a linear stages will give control over the aperture of the DLW by varying the gap between the two slabs. The beam is finally

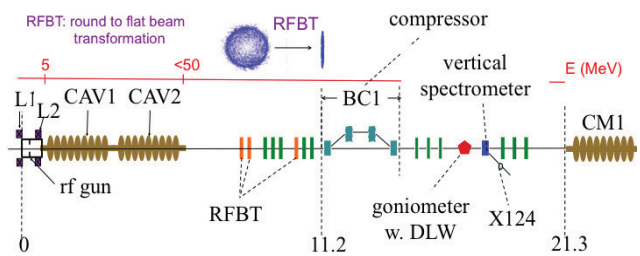

Figure 1: Layout of the ASTA photoinjector. L1 and L2 are solenoids, and CAV1 and 2 SCRF cavities. The green and re rectangles respectively represent normal and skewed quadrupole magnets. X124 is Ce:YAG a screen located in the dispersive section.

drifted to the vertical spectrometer and directed to a Ce:YAG screen (X124) with full vertical size of 38 mm and located at a dispersion of $\eta_y = 0.44$ m permitting the measurement of beam spectrum of $\delta p/p \sim 9$ % relative momentum spread. The high-resolution CCD (Prosilica GC 2450) could in principle enable resolution below $\delta p/p \sim 10^{-4}$ for an ideal zero-emittance beam. The zero-charge betatron functions at X124 viewer are shown in Fig. 2 as a function of betatron functions obtained at the waist ($\alpha_x = \alpha_y = 0$) in the DLW structure. The focusing between the DLW structure and X124 screen is solely achieved by the dipole (no quadrupole magnets are presently installed in this section). For a vertical beta function of $\beta^* \simeq 2$ m at the center of the DLW, the resulting β function at X124 is $\beta_y^{X124} \simeq 1$ m limiting the energy resolution of the spectrometer to 1.8×10^{-4} (for a

* Work supported by the by the Defense Threat Reduction Agency, Basic Research Award # HDTRA1-10-1-0051, to Northern Illinois University and by US DOE contract DE-AC02-07CH11359 to the Fermi research alliance LLC.

ISBN: 978-3-95450-132-8 doi:10.18429/JACoW-IPAC2014-TUPME042

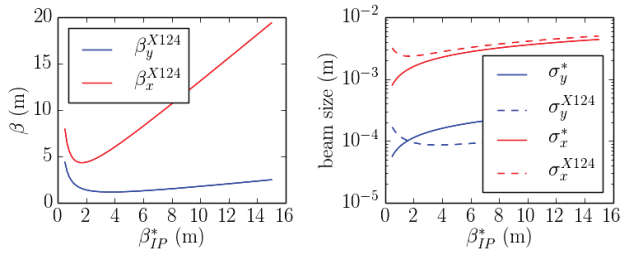

Figure 2: The zero-charge betatron functions (left) and the transverse RMS beam sizes (right) along the ASTA accelerator with flat beams.

geometric emittance of ~ 6.3 nm (corresponding to 0.5 µm normalized with a Lorentz factor $\gamma \simeq 80$).

Finally, a diagnostics station located downstream of the vertical spectrometer will enable the detection and autocorrelation of THz radiation generated by the bunch passing through the DLW structure. The autocorrelation is performed with a Michelson interferometer employing a He-cooled InSb bolometer; see details in Ref. [8].

Our experiment relies on the production of a flat beam, i.e., a beam with large transverse emittance ratio [9]. In our setup we produce flat beams with a low vertical emittance to mitigate horizontal-emittance-dilution effects arising in BC1 via space charge and coherent synchrotron radiation. Another benefit of this configuration is the low betatron contribution to the beam size at X124 given a vertical normalized emittance as low as $\varepsilon_y \simeq 0.3$ µm. An important challenge to overcome is the formation of compressed flat beam as described elsewhere [9].

START-TO-END SIMULATIONS

The start-to-end simulations detailed below were performed using particle-in-cell beam-dynamics program including ASTRA [10] and IMPACT-T [11]. The distribution downstream of the compressor was then matched to a waist at the DLW structure location with ELEGANT [12]. To model the beam self-interaction with its wakefield in the DLW, we use a modified version of IMPACT-T described in Ref. [6]. The dielectric-wakefield model is based on a 3-D Green's function approach and was successfully benchmarked against particle in cell finite-difference time-domain simulations [6]. We consider a DLW structure composed of two parallel dielectric slabs. The separation between the inner surface and outer (metallized) surfaces is respectively $2a$ and $2b$. The dielectric thickness is $b - a$ and its relative permittivity is taken to be $\varepsilon_r = 5.7$ to correspond to diamond.

Case of Single-mode DLW Structures

Single-mode structures have the advantage to produce sinusoidal fields with known wavelengths. However since the beam's energy couples to a single mode, the resulting accelerating fields are generally smaller than the accelerating gradients achieved in multimode structures.

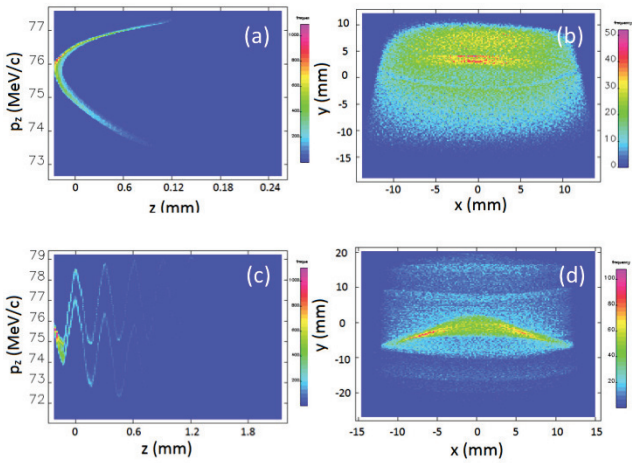

Figure 3: Longitudinal phase spaces (a,c) and associated transverse distributions at X124 (b,d) with (a,b) and without (c,d) a DLW structure. The DLW structure used for (c,d) has parameters a=100 µm, $b = 120$ µm, and $\varepsilon_r = 5.7$.

Due to the limited measurement apparatus in the planned experiment, we must establish a method of decoding the information from the projected energy modulated beam onto X124. Figure 3(a,b) illustrates the nominal longitudinal phase space (LPS) and the associated transverse beam distribution at the X124 location when no DLW structure is inserted in the beam path.

A complication arising from the relatively long photocathode laser pulse (rms duration $\sigma_t \simeq 3$ ps)regards the accumulation of a strong quadratic distortion on the LPS during acceleration in CAV1 and CAV2 which, after bunch compression results in a highly distorted distribution. The distribution has some benefits to the investigation of wakefields as the charge concentration in the bunch head lead to high peak current (~ 5 kA) that excites strong wakes while the long trailing electron population samples this wake over several periods. This feature is clearly demonstrated in Fig. 3(c) where the LPS immediately downstream of a DLW structure with parameters a=100 µm, $b = 120$ µm, and $\varepsilon_r = 5.7$ is shown. The resulting transverse distribution on X124 shows some horizontal bands that correspond to the local maxima of the observed energy modulations on the LPS. Because of the large number of modulations, some smearing occurs at X124. In addition, we note that the Cherenkov pattern resulting from the dependence of the accelerating field on the transverse coordinates can be clearly resolved at X124 and could provide insightful measurements for precise benchmarking of the 3-D model.

Case of Multi-mode DLW Structures

The high-peak current and narrow width of the bunch head is capable of exciting has a spectrum that extents close to 10 THz. It is therefore capable to excite higher-order modes possibly supported by the DLW structure. A simple way to enable multi-mode operation of DLW structures consists

ISBN: 978-3-95450-132-8 doi:10.18429/JACoW-IPAC2014-TUPME042

of using of thicker dielectric thicknesses. Additionally, a thicker thickness can also lead to higher accelerating fields in the DLW as multiple modes can constructively add up. The draw back being the lack of control on the superposition of the mode which can possibly lead to accelerating field region with smaller longitudinal extend compared to single-mode structures. Such a lack of control could lead to the acceleration of witness bunches with distorted LPS or would require very short witness bunches.

Figure. 4 shows examples of LPS and transverse beam distribution simulated at X124 for two dielectric structures with inner radius $a = 100$ µm and outer radius $b = 150$ and 200 µm. The experimental advantage for using multimode structures are the lower number of energy modulations which leads to fewer (and brighter) energy (horizontal) bands at X124.

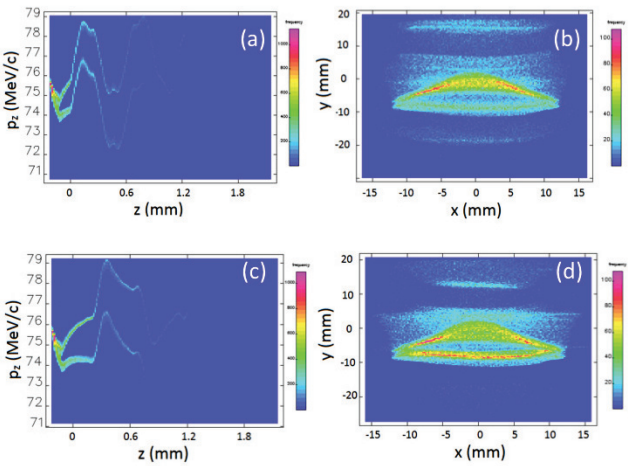

Figure 4: Longitudinal phase spaces (a,c) and associated transverse distributions at X124 (b,d) for a dielectric thickness of $\tau = 50$ (a,b) and 100 µm (c,d) DLW structure. The DLW structure other parameters are $a = 100$ µm, $b = a + \tau$, and $\varepsilon_r = 5.7$.

For the case of multimode structures the peak accelerating field are 110 and 120 MV/m for respectively a dielectric thickness of $\tau = 50$ [Fig. 4(a,b)] and 100 µm [Fig. 4(c,d)] while the single-mode structure was supporting a field amplitude of 105 MV/m [Fig. 3(c,d)]. We finally note that using a flatter beam could allow for smaller inner-aperture structure which could lead to larger accelerating fields. Another path to high axial field is the production of flat beams with higher peak current. This latter possibility would rely on the use of an enhanced compression scheme employing a high-harmonic accelerating cavity [13] or wakefield linearizer [14, 15] to linearizer the bunch's LPS prior to the BC1 chicane. Ultimately, given limited vertical aperture of the X124 screen (38 mm), the measurement of larger accelerating gradients would rely on the use of shorter DLW structures or lower-charge bunches.

CONCLUSION & OUTLOOK

We have demonstrated that ASTA could support tests of beam-driven acceleration based on a slab-symmetric DLW structure driven by flat beams leading to accelerating gradients larger than 100 MV/m.

We note that a possible extension will be the incorporation of longitudinally shaped bunches which could enhance the transformer ratio. Several techniques are currently under consideration ranging from transverse-to- longitudinal phase space exchanger [16], ad initio laser pulse shaping [17], and wakefield-induced shaper combined with ballistic compression [18]. These different techniques, foreseen to be available at ASTA, range in their achieved precision of the control and in their complexity. These scheme will be throughly investigated at ASTA.

REFERENCES

[1] P. Piot et al, Proc. IPAC 14, TUPME041 (2014).

[2] for updated information see http://asta.fnal.gov

[3] P. Piot, et al., Proc. IPAC10, 4316 (2010).

[4] P. Piot, et al. Proc. IPAC13, 2003 (2013).

[5] C. Prokop, et al. Proc. IPAC13, 3103 (2013).

[6] D. Mihalcea, et al., Phys. Rev. ST AB **15**, 081304 (2012).

[7] Y.-M. Shin, et al., Proc. IPAC14, TUPME061 (2014).

[8] Y.-E Sun, et al, Phys. Rev. Lett. **105**, 234801 (2010).

[9] J. Zhu, et al., prepr. Fermilab-PUB-14-103-AD-APC (2014).

[10] K. Flöttmann, ASTRA *User's Manual*, http://www.desy.de/~mpyflo/AstraDokumentation.

[11] J. Qiang, et al., Phys. Rev. ST AB **9**, 044204 (2006).

[12] M. Borland, Advanced Photon Source LS-287, September 2000, available from Argonne National laboratory (2000).

[13] K. Flöttmann, et al., DESY report TESLA-FEL-2001-06 (2001).

[14] P. Craievich, Phys. Rev. ST AB **13**, 034401 (2010).

[15] M. Venturini, "longitudinal phase space linearizer using wakefield in a corrugated beam pipe", private communication; also at the 2nd ASTA users' meeting asta.fnal.gov (2014).

[16] P. Piot, et al., Phys. Rev. ST AB **14**, 022801 (2011).

[17] F. Lemery, et al., Proc. IPAC14, TUPME043 (2014).

[18] F. Lemery, et al., submitted (2014).